iScience

Article

Spatial transcriptomics identifies RBM39 as a gene associated with Gleason score progression in prostate cancer

Graphical abstract

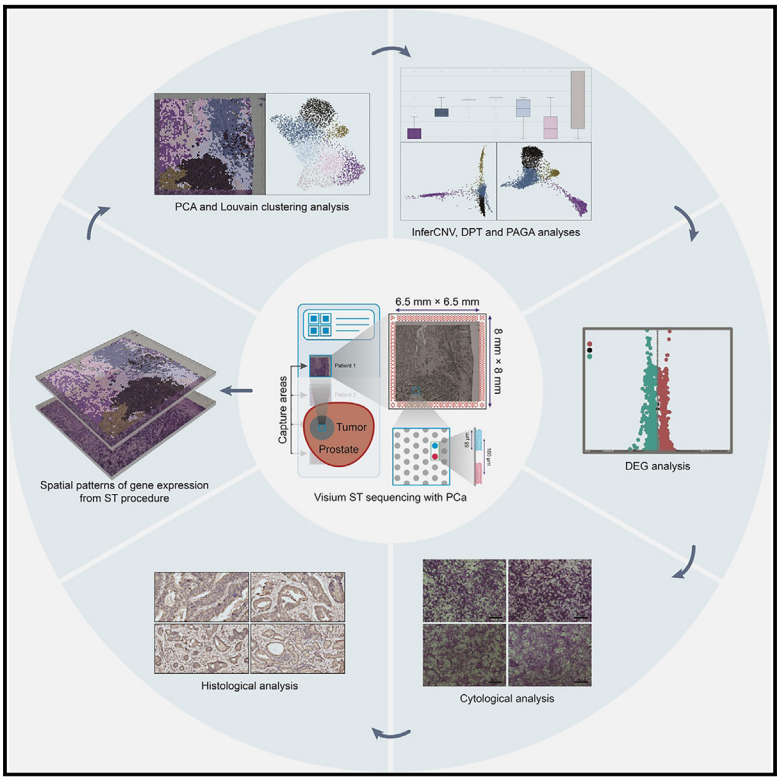

Highlights

- Visum spatial Transcriptomics reveals developmental trajectories of prostate cancer
- Evaluated key genes associated with Gleason score (GS) progression
- Confirmed RBM39 is linked to gradual changes in the GS

Authors

Yongjun Quan, Mingdong Wang, Hong Zhang, Dan Lu, Hao Ping

Correspondence

taotao@bjmu.edu.cn (D.L.), pinghaotrh@ccmu.edu.cn (H.P.)

In brief

Health sciences; Medicine; Cancer

Quan et al., 2024, iScience *27*, 111351
December 20, 2024
https://doi.org/10.1016/j.isci.2024.111351

CellPress

iScience

CellPress
OPEN ACCESS

Article

Spatial transcriptomics identifies RBM39 as a gene associated with Gleason score progression in prostate cancer

Yongjun Quan,[1] Mingdong Wang,[1] Hong Zhang,[2] Dan Lu,[3,*] and Hao Ping[1,4,*]
[1]Department of Urology, Beijing Tongren Hospital, Capital Medical University, Beijing 100176, P.R. China
[2]Department of Pathology, Beijing Tongren Hospital, Capital Medical University, Beijing 100176, P.R. China
[3]Institute of Systems Biomedicine, Department of Immunology, School of Basic Medical Sciences, NHC Key Laboratory of Medical Immunology, Beijing Key Laboratory of Tumor Systems Biology, Peking University, Beijing 100191, P.R. China
[4]Lead contact
*Correspondence: taotao@bjmu.edu.cn (D.L.), pinghaotrh@ccmu.edu.cn (H.P.)
https://doi.org/10.1016/j.isci.2024.111351

SUMMARY

Prostate cancer (PCa) exhibits significant intratumor heterogeneity, frequently manifesting as a multifocal disease. This study utilized Visium spatial transcriptomics (ST) to explore transcriptome patterns in PCa regions with varying Gleason scores (GSs). Principal component analysis (PCA) and Louvain clustering analysis revealed transcriptomic classifications aligned with the histology of different GSs. The increasing degree of tumor malignancy during GS progression was validated using inferred copy number variation (inferCNV) analysis. Diffusion pseudotime (DPT) and partition-based graph abstraction (PAGA) analyses predicted the developmental trajectories among distinct clusters. Differentially expressed gene (DEG) analysis through pairwise comparisons of various GSs identified genes associated with GS progression. Validation with The Cancer Genome Atlas Prostate Adenocarcinoma (TCGA-PRAD) dataset confirmed the differential expression of RBM39, a finding further supported by cytological and histological experiments. These findings enhance our understanding of GS evolution through spatial transcriptomics and highlight RBM39 as a gene associated with GS progression.

INTRODUCTION

Prostate cancer (PCa) is recognized as a multifocal disease occurring within a single gland.[1,2] Recent studies have indicated that intratumor heterogeneity in multifocal PCa arises from a monoclonal disease, with each lesion representing a distinct stage in the evolutionary process.[3–7] Thus, understanding the genetic patterns among multiple lesions can help us trace the origins and triggers of PCa progression.

The origin of multifocal PCa has been extensively reported, suggesting that glandular epithelial (GE) cells, such as basal and luminal cells, serve as the source cells for PCa.[8–14] In prostate tissue, PCa is diffusely distributed with multiple foci, often mixed with non-glandular tissue such as the anterior fibromuscular stroma (AFMS). Precisely determining the genetic expression profiles of GE cells poses a major challenge in the transcriptomic analysis of PCa.

Since PCa does not exhibit a clear macroscopic boundary that distinguishes it from normal GE cells or non-glandular tissues, accurately extracting transcriptome information presents a significant challenge in PCa analysis. Single-cell sequencing technology has been utilized to detect intratumor transcriptome heterogeneity at the level of individual cells and to search for molecular events during the transdifferentiation to advanced malignant stages of PCa.[15–17] However, this approach lacks spatial information and relies to some extent on inferences made from bioinformatics.[18,19] While in situ sequencing techniques can confirm the histological structures of the target area, they are limited to measuring small numbers of specific genes.[20,21]

Spatial transcriptomics (ST) offers a distinct advantage by combining high-throughput RNA sequencing analysis with the examination of spatial information and the histological context of tissues. This technique allows researchers to comprehensively correlate transcriptome-wide expression patterns with specific spatial distributions and morphological features of the tissue, which provides a richer biological context.[7,22–25] Visium ST analysis, renowned for its high spatial resolution, utilizes microarrays containing 4,992 spatially barcoded spots, each measuring 55 μm in diameter, within capture areas of 6.5 × 6.5 mm^2. This approach provides high-throughput gene expression data, making it invaluable for large-scale studies and the discovery of new biological insights, and represents an optimal method for identifying distinct histological structures.[7,25]

To analyze multifocal PCa, a fundamental prerequisite is the standardized assessment of each lesion at the progression stage using hematoxylin-eosin (H&E)-stained histological images. Currently, the Gleason grading system serves as the

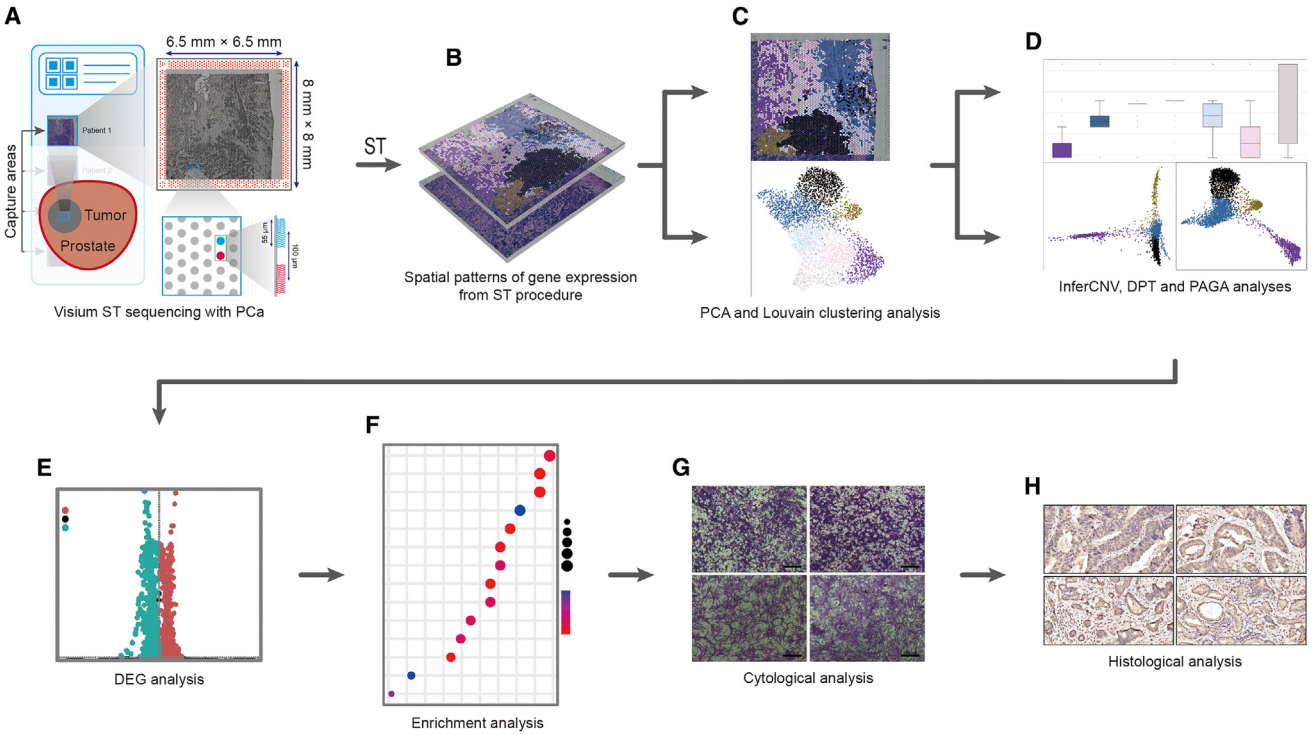

Figure 1. Workflow of this study

(A) Visium ST analysis was conducted by placing PCa tissue on a Visium Spatial slide, which contained a microarray of 4992 spatially barcoded spots within capture areas measuring 6.5 × 6.5 mm^2.

(B) Matrices of read counts for the full transcriptome in each spot were obtained through genomic alignment.

(C) The spots in the PCa section were categorized into distinct groups using PCA and Louvain clustering analysis and were then annotated as GE with a specific GS or as AFMS based on histological structures.

(D) InferCNV, DPT, and PAGA analyses were performed to assess the malignancy and developmental trajectories of distinct tissue types identified by histology.

(E) DEG analysis was performed by comparing the data on the basis of the GS progression pattern.

(F) The DEGs subsequently underwent enrichment analyses to assess their biological functions during GS progression.

(G and H) The mRNA and protein expression encoded by the identified gene RBM39 in various PCa cells and tissues was validated through cytological (G) and histological (H) analyses.

most reliable system for evaluating pathological stage and disease progression in PCa.[26–28] This system enables the prediction of PCa malignancy and provides prognostic outcomes, including extraprostatic spread, biochemical recurrence, and overall patient survival.[29–34]

In this study, we utilized a PCa tissue sample and employed Visium ST to analyze the transcriptome-wide expression profiles of the PCa section with varying Gleason scores (GSs). Through this analysis, we identified key genes and biological implications associated with GS progression. Ultimately, we identified an essential gene associated with PCa malignancy—RNA-binding motif protein 39 (RBM39), which was further validated through cytological and histological experiments.

RESULTS

Workflow of the Visium spatial transcriptomics analysis

The workflow of the ST analysis is illustrated in Figure 1. The spatial microarray comprised 4992 distinct barcoded spots within the capture areas measuring 6.5 × 6.5 mm^2. Each spot contained extensive transcriptome-wide information representing the entire genome (Figures 1A and 1B). Principal component analysis (PCA) was applied to reduce the dimensionality of the spots, followed by Louvain clustering analysis to categorize them into various groups, namely GE tissues with a specific GS and AFMS tissues (Figure 1C). Several bioinformatic analyses, including inferred copy number variation (inferCNV), diffusion pseudotime (DPT), and partition-based graph abstraction (PAGA) analyses, were subsequently performed to evaluate the malignancy stages and developmental trajectories of distinct tissue types identified by histology (Figure 1D). To explore genes associated with PCa progression, differentially expressed gene (DEG) analysis was conducted through comparisons on the basis of the GS progression pattern (Figure 1E). The selected DEGs were subjected to enrichment analyses, including Gene Ontology (GO) and Kyoto Encyclopedia of Genes and Genomes (KEGG) analyses, to elucidate their biological roles in the progression of GS (Figure 1F). Additionally, the differential mRNA and protein expression encoded by the selected gene RBM39 in various PCa cells and tissues was validated through cytological and histological analyses (Figures 1G and 1H).

Table 1. Clinicopathological characteristics of selected patients with PCa for ST analysis

Age	TPSA (ng/mL)	FPSA/TPSA	GS (biopsy)	GS (pathology)	pT stage	ISUP grade	AJCC stage
65	23.91	0.1	3 + 3∼3 + 4	3 + 4	T3b	2	IIIB

TPSA: total prostate specific antigen; FPSA: free prostate specific antigen; GS: Gleason score; pT: pathological T; ISUP: International Association of Urology Pathology; AJCC: American Joint Committee on Cancer.

Transcriptomic heterogeneity of prostate cancer tissue

The patient information for the PCa tissues used in this study for ST analysis is presented in Table 1. Owing to the heterogeneity of GS observed in multifocal PCa,[35] distinct histological structures of GS 3 + 3, 3 + 4, and 4 + 3 within GE cells were annotated through H&E-stained image (Figure 2A). To elucidate the transcriptomic classifications across all the cellular regions, we employed PCA in conjunction with Louvain clustering analysis. These analyses revealed a striking resemblance between the transcriptomic profiles and the histologically identifiable structures of PCa tissues with varying GSs, as well as adjacent tissue termed AFMS (Figure 2B). A GS of 3 + 3 in PCa signifies the presence of well-differentiated cells exhibiting low-grade cellular changes and low capacity for metastasis.[36–38] Consequently, lesions classified as GS (3 + 3) are considered precancerous.[39,40] We investigated clonal hierarchies and tumor malignancy by employing inferCNV analysis with the reference group of GS (3 + 3) lesions.[3–7,16,17] Our findings demonstrated that GS progression was associated with higher median inferCNV scores (Figure 2C). Additionally, unsupervised hierarchical clustering analysis employing inferCNV did not reveal significant differences between the structures of GE cells and AFMS (Figure 2D).

Spatial distributions of gene expression during the progression of Gleason scores

The developmental trajectories of tissues with various GSs were inferred using DPT and PAGA analyses. We observed that clusters associated with GS $\geq$ 7 [GS (3 + 4)_1, GS (3 + 4)_2, and GS (4 + 3)] were densely distributed, indicating highly aggressive diseases.[41,42] The geodesic distances and diffusion map of these clusters along the graph illustrated a certain developmental pattern during the GS upgrading process (Figures 3A and 3B).

To gain deeper insight into the molecular foundations of GS progression, we examined the expression levels of genes related to GS progression by comparing the GS (3 + 4)_1 and GS (3 + 3), GS (3 + 4)_2 and GS (3 + 3), GS (4 + 3) and GS (3 + 4)_1, as well as GS (4 + 3) and GS (3 + 4)_2 (Figure 3C). We identified a total of 61 genes (e.g., KLK2, KLK11, and RBM39) that exhibited a positive correlation with GS upgrading, while 34 genes presented a negative association [with an absolute value of natural logarithm fold change (|ln FC|) > 0.1 and q-value < 0.001 according to the Wilcoxon test] (Figure 3D).

Furthermore, we evaluated the biological functions and signaling pathways involved in GS progression. The enrichment analyses of the overlapping genes among at least 3 out of the 4 comparisons revealed the enrichment of purine ribonucleoside and nucleoside triphosphate metabolic processes (according to GO analysis), as well as oxidative phosphorylation and antigen processing and presentation (according to KEGG analysis) (Figure 3E).

Validation of Gleason score development-related genes using The Cancer Genome Atlas Prostate Adenocarcinoma (TCGA-PRAD) dataset

We then assessed the 72 overlapping genes revealed by the alignment of genomic data from the TCGA-PRAD dataset, which exhibited detectable expression values. These genes were further examined for their expression patterns in patients with TCGA-PRAD classified on the basis of a range of clinicopathological characteristics. Notably, we observed significant dysregulation (p < 0.05 according to the Wilcoxon test) in 64, 21, and 20 genes (represented by KLK2, LBH, LSM7, PILRB, and RBM39) when comparing the tumor and normal samples, GS > 7 and GS < 7 groups, and pathological T3 (pT3) and pT2 stages (Figures 4A–4C; Tables S4–S6). Notably, TP53 aberration serves as a crucial criterion for identifying malignancy in PCa.[43] Accordingly, we analyzed the expression levels of these genes across the TP53 mutation group and the wild-type group and detected differential expression of 22 genes (Table S7).

To evaluate the prognostic impact of the 72 genes, we conducted survival analysis by dividing patients with TCGA-PRAD into two groups on the basis of the optimal cutoff value of gene expression, defined by the minimal log rank p-value from the result of the Kaplan−Meier (K−M) analysis. Our findings indicated that 10 and 16 genes, including GLUD1, PILRB, RBM39, and RGL2, were significantly correlated with recurrence-free survival (RFS) and progression-free survival (PFS), respectively (p < 0.05 in Cox regression analysis). Furthermore, among these genes, 5 and 14 (represented by PILRB, RBM39, and RGL2) were associated with poor prognosis [hazard ratio (HR) > 1 and p < 0.05 in Cox regression analysis] (Figures 4D and 4E; Tables S8 and S9).

We summarized the intersecting genes that exhibited dysregulation across the aforementioned comparisons (p < 0.05) (Figure 4F; Table S10). Interestingly, we detected diverse expression tendencies in genes, such as DEGS1 and ERP29, were related to the GS transition from GS (3 + 3) to GS (4 + 3) in the ST analysis and advanced stages (e.g., tumor, GS > 7, pT3, and TP53 mutation in their respective comparative analyses) as well as poor prognosis (HR > 1 in RFS and PFS analyses) in the TCGA-PRAD dataset. This inconsistency might be ascribed to intratumor heterogeneity and histological atypia of the collected PCa tissues in the TCGA-PRAD dataset, leading to a mismatch between the transcriptome data and the actual pathological diagnosis. Furthermore, we summarized the genes exhibiting a trend that is generally consistent with progression to advanced stages, including PILRB, RBM39, LSM7, RGL2, SNHG7, CCDC85B, CDK5RAP3, and LBH, as evidenced by the ST analysis and TCGA-PRAD dataset (Figure 5A; Table S10). Specifically, the two intersecting genes, PILRB and RBM39, displayed a positive correlation with GS progression according to the ST analysis and were simultaneously elevated in the advanced stages of TCGA-PRAD (Table S10). Spatial activity maps and PAGA graphs

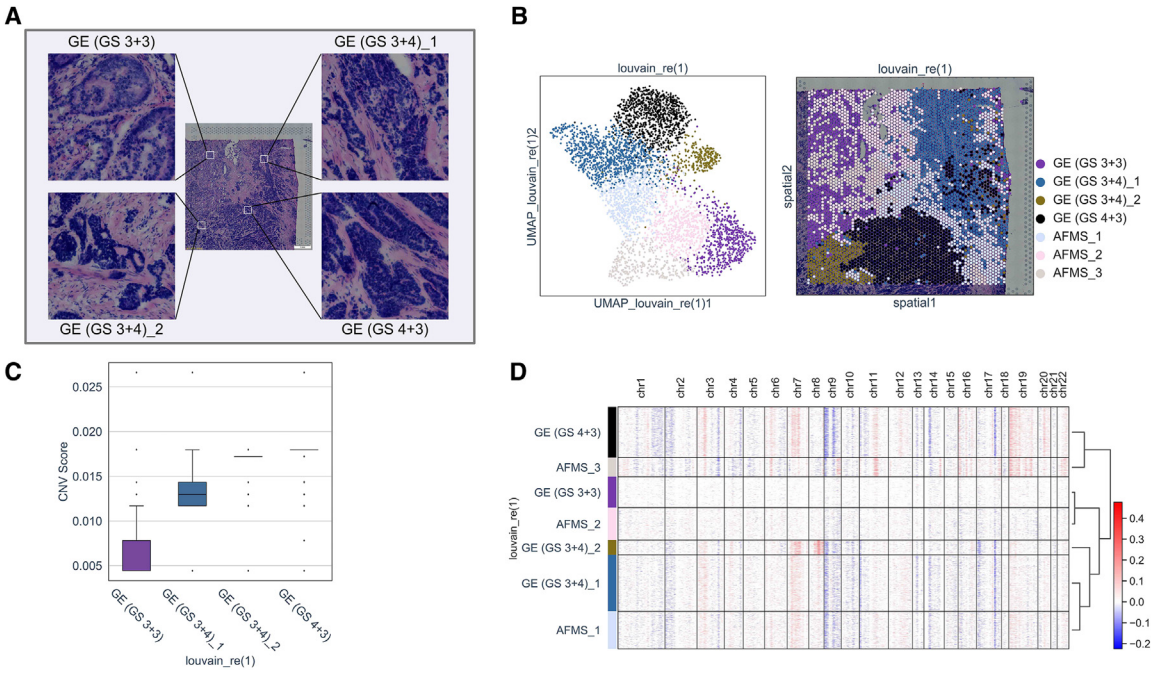

Figure 2. Transcriptomic heterogeneity of PCa tissue

(A) H&E-stained image of the PCa section. Four different histologically identifiable structures are enlarged and annotated with corresponding GSs.

(B) The transcriptomic classifications across all spots were assessed through PCA and Louvain clustering analysis and visualized by UMAP (left). The spots affiliated with clusters overlaid on the histological image were annotated as GE with a specific GS or AFMS according to the histological structures (right).

(C) The median CNV score, along with interquartile range (IQR) for each GE subcluster, was calculated through inferCNV analysis and is displayed in the corresponding boxplot.

(D) The chromosomal landscape based on inferCNV values for distinguishing clusters of GSs and AFMS tissue is shown as a heatmap.

revealed the involvement of these two genes in GS progression (Figures 5B and 5C). Finally, we selected RBM39 and conducted experimental validation through both cytological and histological research on its gene expression.

Knockdown of RNA-binding motif protein 39 suppresses prostate cancer cell proliferation and invasion

To investigate the role of RBM39 in tumorigenesis, we silenced RBM39 expression in C4-2, PC3, and DU145 cells. The effectiveness of the knockdown was confirmed by quantitative PCR (qPCR) and Western blot (WB) analysis (Figures S1A and S1B). We employed various assays, such as Cell Counting Kit-8 (CCK-8), colony formation, wound healing, and Transwell, to assess the impact of RBM39 expression on PCa cell viability. Our results demonstrated that the downregulation of RBM39 expression significantly inhibited the proliferation, migration, and invasion of various PCa cells (Figures 6A–6D).

RNA-binding motif protein 39 protein expression is relatively elevated in advanced-stage prostate cancer tissues

The levels of RBM39 protein expression in prostatic intraepithelial neoplasia (PIN) and PCa tissues were examined via immunohistochemical (IHC) analysis. The clinicopathological characteristics of the patients with PCa included in the IHC analysis are shown in Table 2. The representative IHC-stained images revealed that RBM39 protein expression gradually increased during GS progression (Figure 7A). The percentages of cells displaying RBM39 staining and the staining indices of RBM39 were quantified in PCa tissues stratified by GS (GS < 7, GS = 7, and GS > 7) as well as pT stages (pT2, pT3, and pT4). These values generally increased during both GS and pT progression (Figure 7B). Our findings indicate a positive association between RBM39 protein expression and the progression of PCa to more advanced stages.

DISCUSSION

PCa originates from either luminal or basal cells within the glandular epithelium[8–14] and is surrounded by nonglandular (such as AFMS) tissues. It is a multifocal disease that is diffusely distributed in prostate tissue, making it challenging to distinguish PCa from nonglandular tissues visually. This confusion in pathological diagnosis and transcriptome sequencing analysis poses difficulties in PCa analysis. The discrepancy in partial genes between our ST and TCGA-PRAD analyses supports this observation.

Visium ST technology is particularly suitable for PCa analysis due to its high resolution and ability to comprehensively quantify the entire transcriptome across spatial dimensions. In this study, we analyzed the DEGs in various histological features of GE cells.

To investigate the evolutionary process of PCa, it is important to clarify the origin and relationship of various lesions within a

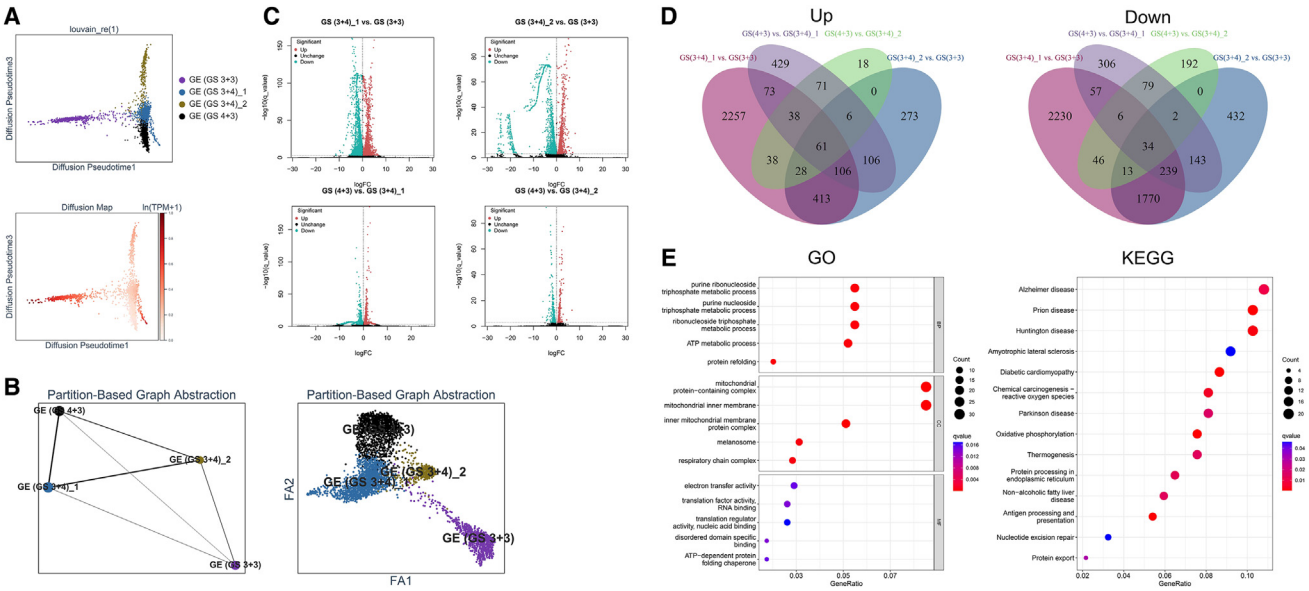

Figure 3. Spatial distributions of gene expression during the progression of GS

(A) The appropriate coordinates of the tumor regions of different GSs (top) were constructed through DPT analysis, and the diffusion map of dpt_pseudotime (bottom) was used to infer the development path.

(B) The GS developmental trajectory map was inferred on the basis of retaining the GE subclusters (left) and each spot (right) through static PAGA graphs.

(C) DEG analysis of the comparisons among GS (3 + 4)_1 and GS (3 + 3), GS (3 + 4)_2 and GS (3 + 3), GS (4 + 3) and GS (3 + 4)_1, as well as GS (4 + 3) and GS (3 + 4)_2 was visualized in volcano plots.

(D) The numbers of genes that were simultaneously upregulated (left) or downregulated (right) during GS upregulation are summarized in Venn diagrams.

(E) Genes simultaneously included in $\geq$ 3 of the 4 comparisons were subjected to GO (up) and KEGG (down) enrichment analyses, the results of which are shown in bubble plots. BP: biological process; CC: cellular component; MF: molecular function.

single sample. Acquired partial genomic aberrations trigger the advancement of PCa to later stages and the formation of multiple distinct phenotypes of subclones.[3–7,44,45] Researchers have conducted high-resolution genome-wide analysis and discovered that cells from separate foci of PCa can be traced back to a single genomically aberrant cell with the same allele-specific CNV values.[3,4,7] Therefore, disparate lesions from multifocal PCa may emerge from a single PCa precursor[3–7] through an ongoing Darwinian evolutionary process.[46,47]

The current study operates on the premise that the heterogeneity of GS among different regions of a single tumor represents diverse developmental stages of tumor cells that evolved from a monoclonal origin. Previous research revealed that the spatial profiles of factor activity determined by ST analysis closely mirrored the profiles of factors identified by immunostaining and analysis of histologically identifiable structures; PCA confirmed the clear separation among structures of the normal prostate, GS 3 + 3, and PIN.[22] Therefore, we classified the spots within the PCa sections into different histological structures through PCA and Louvain clustering analysis.

Unlike the methods used in our previous study,[25] we utilized highly variable genes (HVGs) instead of all genes for PCA. HVGs exhibit highly dynamic expression patterns across all spots, and these variations are more likely to be biologically relevant. Using HVGs reduces the influence of technical noise, making PCA more reflective of true biological differences and thus better candidates for differentiating among various histological structures. HVGs in this study typically constitute only a small subset of all genes, characterized by a minimum mean of 0.0125, a maximum mean of 3, a minimum dispersion of 0.5, and a maximum dispersion of 1000, which significantly improves computational efficiency. Consequently, using HVGs for PCA usually results in clearer and more meaningful clustering, as these genes contain more differential information and are not dominated by background noise. As anticipated, the subgroups overlaid on the H&E-stained histological image generally corresponded to GSs of 3 + 3, 3 + 4, and 4 + 3.

Next, we evaluated the accuracy of the macroscopic assessment of tumor histologic features through computational analysis in bioinformatics. The mean value of inferCNV was reported to serve as the criterion for identifying the malignancy of PCa cells.[16,17] We evaluated PCa malignancy through inferCNV analysis to verify our previous annotation of different GSs. GS (3 + 3) is well differentiated and metastasis free[41] and is regarded as a precancerous lesion.[39] Without "normal" GE cells in our PCa section, we considered GS (3 + 3) as a reference group for inferCNV analysis to compare the expression among the genomic regions. In accordance with our expectation, the median inferCNV values progressively increased during the advancement of the GS. We further reconstructed the developmental trajectories of tumor regions of different GSs using DPT and PAGA analyses. Our findings indicated that the geodesic distances and diffusion map across the graph generally illustrated the development process associated with GS upgrading. These analyses confirm that the study of our visual histological assessment and genetic validation is logical and accurate.

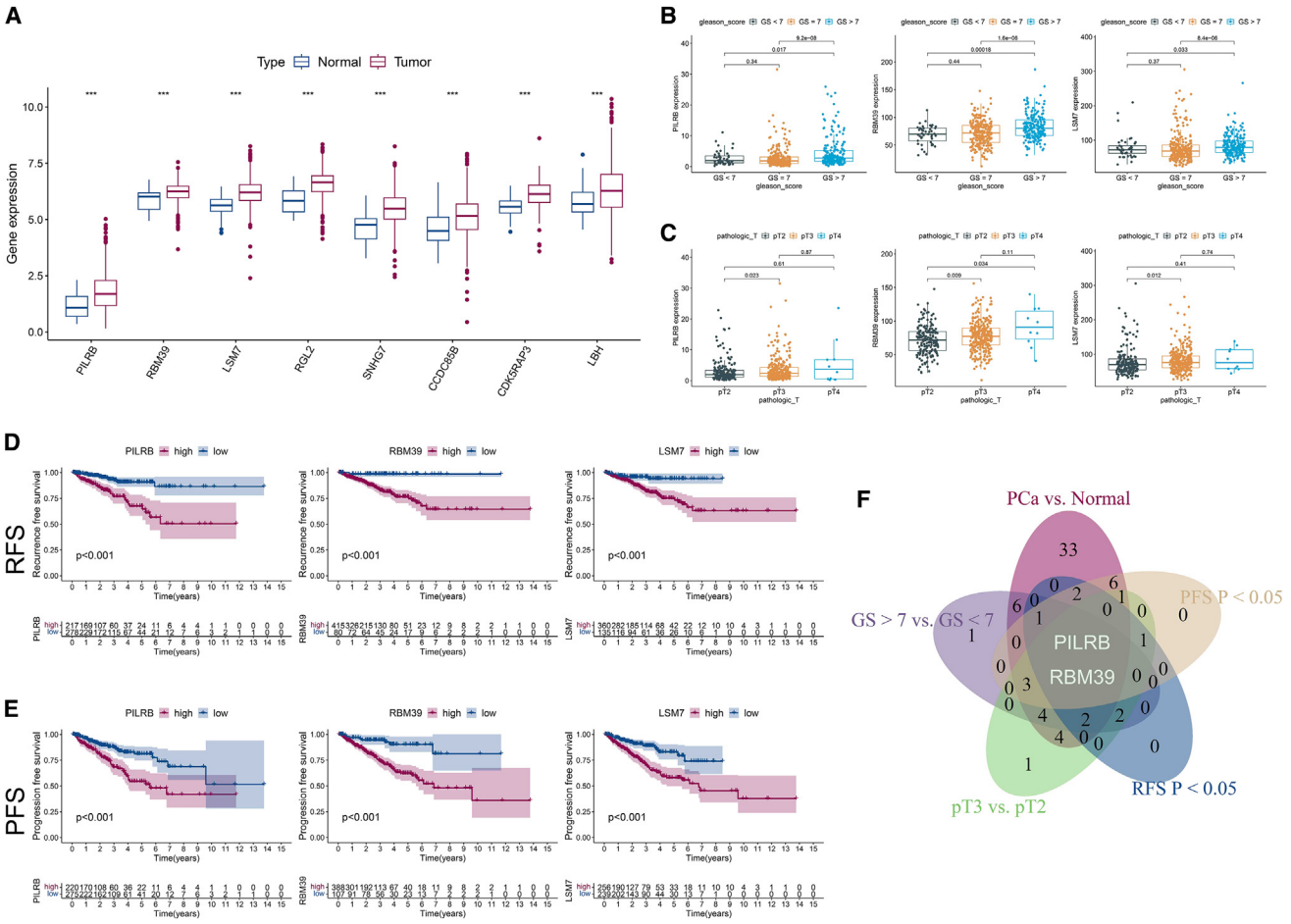

Figure 4. Validation of the GS development-related genes using the TCGA-PRAD dataset

(A) The genes with generally coincident tendency in the advanced stages according to the TCGA-PRAD and ST analyses are summarized in Table S10. The expression levels of these genes in PCa and normal prostate tissues in the TCGA-PRAD dataset are shown in a boxplot. The median and IQR are shown. ***$p < 0.001$.

(B and C) Distribution of the 3 representative genes (PILRB, RBM39, and LSM7) across tumor regions with different GSs (GS < 7, GS = 7, and GS > 7) (B) and pT stages (pT2, pT3, and pT4) (C) in the TCGA-PRAD dataset is shown in the boxplots. The median and IQR are shown. *p*-values from the Wilcoxon test are presented above each pair of comparisons.

(D and E) Survival analysis was performed with the prognostic outcomes of RFS (D) and PFS (E) for the 3 genes by dividing patients with TCGA-PRAD into two groups according to the optimum cutoff. The results are shown as K–M survival curves with *p*-values and the numbers at risk.

(F) The intersecting genes in the above comparisons ($p < 0.05$ in the Wilcoxon test or Cox regression analysis) are shown in a Venn diagram.

After the preliminary determination of the degree of tumor malignancy and developmental trajectories in our annotated GS clusters, we investigated GS progression-related genes through pairwise comparisons corresponding to GS progression. DEGs that were common to at least 3 of the 4 comparisons were subjected to enrichment analysis, which revealed that biological functions such as purine ribonucleoside and nucleoside triphosphate metabolic processes were potentially associated with progression according to the GS.

The identified DEGs were subsequently evaluated for their associations with clinicopathological parameters and prognosis in the TCGA-PRAD dataset and was found that the levels of genes such as PILRB, RBM39, LSM7, RGL2, and SNHG7 were consistently associated with advanced stages across both the ST and TCGA-PRAD analyses. In particular, the intersecting genes PILRB and RBM39 were simultaneously upregulated during the progression of GS [from GS (3 + 3) to GS (4 + 3)] in the ST analysis, and at all of the advanced stages (tumor, GS > 7, pT3, TP53 mutation, and HR > 1 in their respective comparative analyses) from the TCGA-PRAD dataset.

PILRB (paired immunoglobulin-like type 2 receptor β) reportedly regulates inflammatory responses to pathogen infection and significantly contributes to host disease resistance and susceptibility.[48] It interacts with the ligand CD99 to epithelial cells and migrates immune cells to sites of inflammation to trigger the innate immune response.[49] In PCa, the PILRB level was significantly increased in high-risk patients with PCa .[50] However, the specific molecular mechanism and signaling pathway underlying this association are unclear.

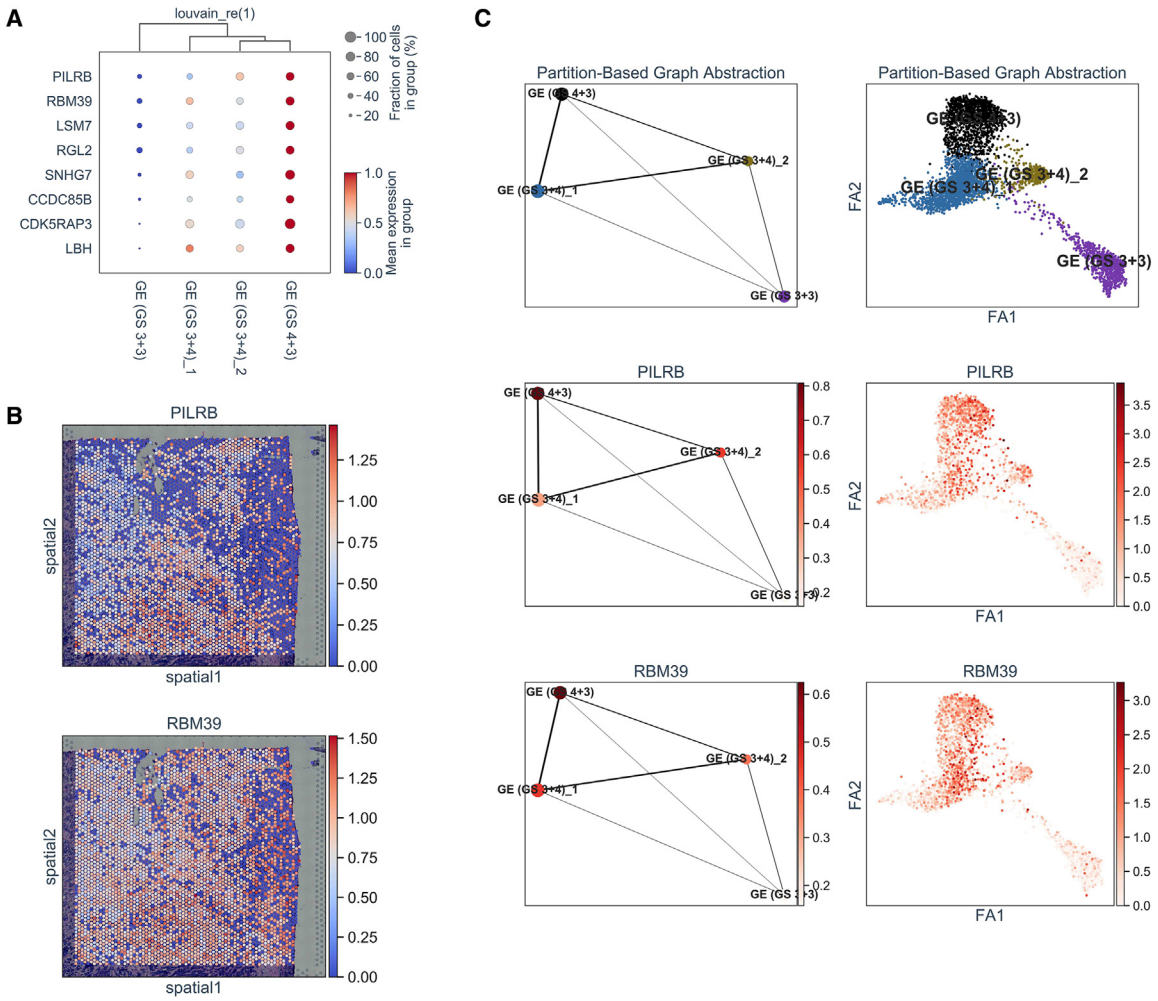

Figure 5. Expression patterns of crucial genes during GS progression

(A) The genes presented in Figure 4A are enumerated, and the relative expression levels of these factors across varying GSs are shown in the bubble plot.

(B) The expression patterns of the simultaneously altered genes PILRB and RBM39 are shown in spatial activity maps in the histological image.

(C) The expression levels and distribution of the 2 genes on the basis of the GE subclusters (left) and spots (right) are shown in the PAGA graphs.

RBM39 (RNA-binding motif protein 39) is a member of the U2 auxiliary factor (U2AF)-like family of proteins closely associated with key splicing factors, such as U2F 65 kDa subunit (U2F65) and poly(U)-binding splicing factor 60 (PUF60).[51,52] Studies using global transcriptomic data confirmed that RBM39 is essential for alternative splicing of a wide range of pre-mRNAs.[53–56] RBM39 is highly expressed in multiple types of cancers, and its functional depletion leads to the simultaneous disruption of transcriptional regulation pathways via large-scale splicing defects in cancer cells.[57,58] In the present study, cytological and histological experiments confirmed the enhancing effect of RBM39 mRNA on PCa cell proliferation, migration, and invasion and the progressive increase in RBM39 protein expression during GS and pT upgrading. In PCa, androgen receptor (AR) variant 7 (AR-V7) is associated with resistance to AR signaling inhibitors (ARSi),[59–61] and RBM39 is essential for alternative splicing of AR-V7 mRNA transcripts derived from AR pre-mRNA.[62] However, another study reported that RBM39 is downregulated in enzalutamide-resistant PCa cell lines compared with sensitive cells,[63] therefore, further research to verify the specific role of RBM39 in castration-resistant PCa (CRPC) progression is warranted.

RBM39 is also involved in transcriptional coregulation[57,58] and mediates transactivation by increasing the functions of several transcription factors, such as estrogen receptor-α/β (ERα/β),[51] the c-Jun component of activating protein-1 (AP-1),[64] and NF-κB.[65,66] Additionally, RBM39 was reported to form an epigenomic regulatory complex by interacting with JMJD6[67] and MLL1,[68] which co-occupy target gene promoters, to disrupt gene transcription via histone 3 lysine 4 (H3K4) trimethylation (H3K4me3) and induce cancer cell proliferation. In triple-negative breast cancer (TNBC), suppression of the interaction between RBM39 and c-Jun was reported to inhibit cell proliferation, highlighting the importance of RBM39-mediated AP-1 activation in TNBC progression.[69] Our previous study revealed that c-Jun interacts with AR and binds to the promoter of NDRG1 to suppress NDRG1 transcription through DNA hypermethylation,

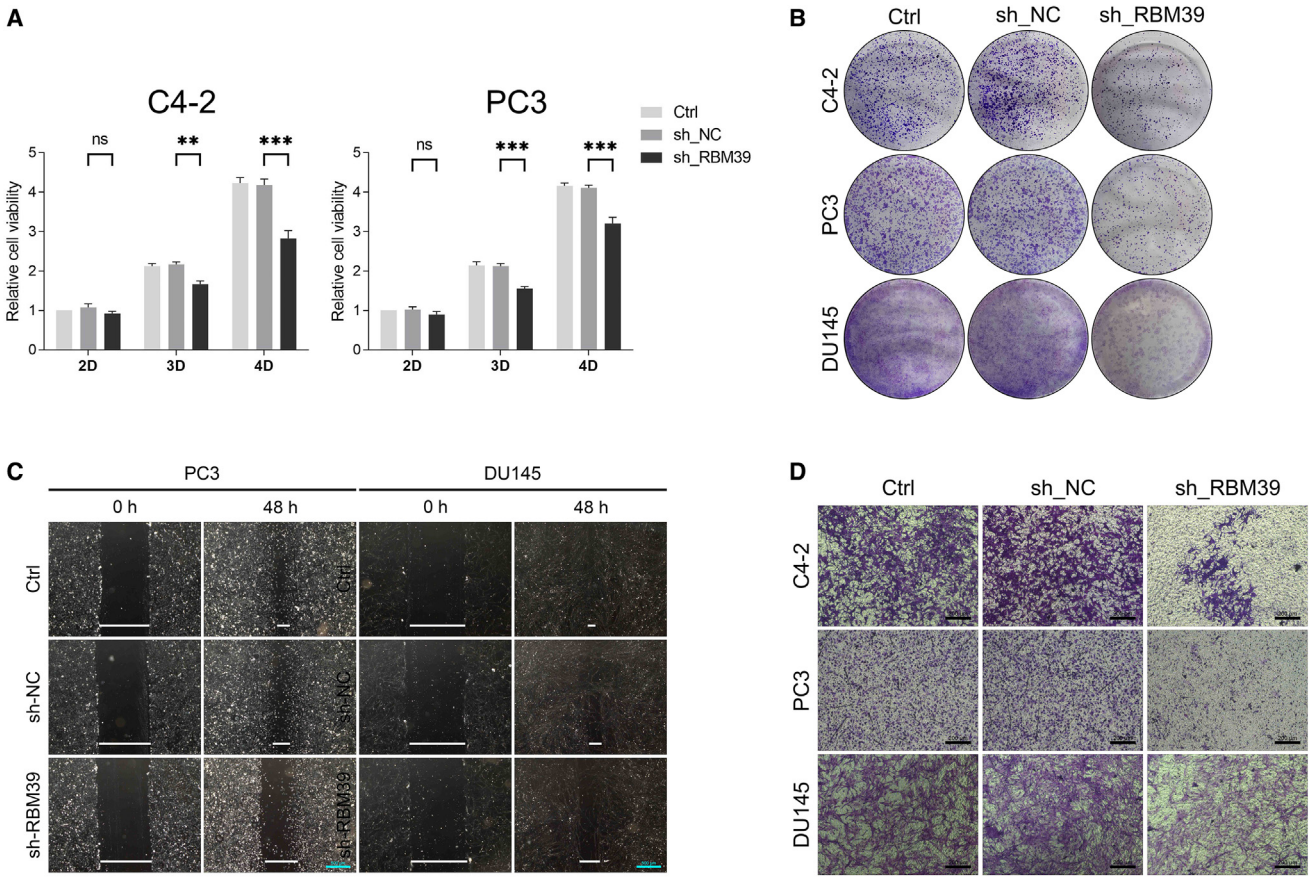

Figure 6. Knockdown of RBM39 gene expression inhibits PCa cell proliferation, migration, and invasion

(A–D) RBM39 expression was knocked down in C4-2, PC3, and DU145 cells. Subsequently, cell proliferation, migration, and invasion were evaluated in 2 or 3 PCa cell lines using CCK-8 (A), colony formation (B), wound healing (C), and Transwell (D) assays. The means ± standard errors of the means (SEMs) are displayed in the histograms of CCK-8 analysis. ns $p > 0.05$; ** $p < 0.01$; and *** $p < 0.001$. Ctrl: the parental cells; sh_NC: negative control cells; sh_RBM39: RBM39 stably downregulated cells.

further inducing PCa progression and castration resistance.[70] RBM39, a coactivator of c-Jun, may affect the c-Jun/NDRG1 axis during PCa progression.

Conclusions

In this study, we employed Visium ST technology to accurately assess the transcriptome-wide expression profiles of GE cells at a high spatial resolution. Our results revealed developmental trajectories and altered gene expression patterns during PCa cell progression. By comparing different GE cell clusters and validating them with the TCGA-PRAD dataset, we identified DEGs associated with GS progression, such as PILRB and RBM39. Furthermore, we confirmed the enhancing effect of RBM39 on PCa progression through cytological and histological experiments. Overall, this study provides valuable insights into ST-based PCa cell evolution and identifies RBM39 as a gene related to GS progression.

Limitations of the study

Several limitations are present in this study. First, we used only a single PCa tissue sample for ST analysis, which inevitably led to errors caused by individual heterogeneity. Second, we found two GS (3 + 4) clusters with different transcriptome expression patterns, implying that there is intratumor heterogeneity in PCa even within the same GS, which limits the determination of representative and universal gene expression patterns in GS (3 + 4). Finally, the signaling pathways and molecular mechanisms affected by RBM39 in PCa warrant further experimental clarification.

RESOURCE AVAILABILITY

Lead contact

Further information and requests for resources and reagents should be directed to and will be fulfilled by the lead contact, Hao Ping (pinghaotrh@ccmu.edu.cn).

Material availability

This study did not generate new unique reagents.

Data and code availability

- This article analyzed existing, publicly available data. These accession numbers for the datasets are listed in the key resources table.
- This article does not report the original code.

Table 2. Clinicopathological characteristics of patients with PCa for IHC analysis

Clinicopathological parameters	Total (n = 45)
Age	
Median age, year (IQR)	68 (64.5–72.5)
Range, year (Min, Max)	54–83
Number of age category, n (%)	
<65	11 (24.4)
≥65	34 (75.6)
Pre-RP t-PSA level	
Median, ng/ml (IQR)	7.6 (5.95–20.6)
Range, ng/ml (Min, Max)	0.2–149
Number of t-PSA status, n (%)	
<4 ng/mL	4 (8.9)
4-10 ng/mL	22 (48.9)
10-20 ng/mL	7 (15.6)
>20 ng/mL	12 (26.7)
f-PSA/t-PSA (f/t)	
Median (IQR)	0.101 (0.1–0.185)
Range (Min, Max)	0.065–0.5
Number of f/t status, n (%)	
<0.16	31 (68.9)
≥0.16	14 (31.1)
Number of total GS status, n (%)	
<7	11 (24.4)
=7	16 (35.6)
>7	18 (40.0)
Number of pT stage, n (%)	
T2	21 (46.7)
T3a	13 (28.9)
T3b	4 (8.9)
T4	7 (15.6)
Number of ISUP grade, n (%)	
1	11 (24.4)
2	11 (24.4)
3	5 (11.1)
4	8 (17.8)
5	10 (22.2)
Number of AJCC stage, n (%)	
I	7 (15.6)
IIA	3 (6.7)
IIB	7 (15.6)
IIC	2 (4.4)
IIIA	2 (4.4)
IIIB	14 (31.1)
IIIC	10 (22.2)

IQR: Interquartile range; RP, radical prostatectomy; t-PSA: total prostate-specific antigen; f-PSA: free prostate-specific antigen; GS: Gleason score; pT: pathological T; ISUP: International Association of Urology Pathology; AJCC: American Joint Committee on Cancer.

- Any additional information required to reanalyze the data reported in this article is available from the lead contact upon request.

ACKNOWLEDGMENTS

This work was supported by the National Natural Science Foundation of China (Grant Nos. 82072833 and 82272864 to Hao Ping) and by the Capital's Funds for Health Improvement and Research (No. 2024-2-2059 to Hao Ping).

AUTHOR CONTRIBUTIONS

The study was designed by Hao Ping, Dan Lu, and Yongjun Quan. Hao Ping supplied the clinical PCa tissue samples, while Mingdong Wang collected them. Yongjun Quan conducted the bioinformatic analysis and, along with Mingdong Wang, performed the cytological and histological experiments. Hong Zhang performed the pathological diagnosis. Yongjun Quan and Dan Lu wrote the article, which was approved by all the authors.

DECLARATION OF INTERESTS

The authors declare that they have no competing interests.

STAR★METHODS

Detailed methods are provided in the online version of this paper and include the following:

- KEY RESOURCES TABLE
- EXPERIMENTAL MODEL AND STUDY PARTICIPANT DETAILS
  - Preparation of prostate cancer (PCa) tissues
  - Cell culture
  - Ethical statement
- METHOD DETAILS
  - Visium spatial transcriptomics (ST)
  - Gene regulation in PCa cell lines
  - Reverse transcription (RT) and quantitative real-time PCR (qPCR) analysis
  - Western blotting (WB)
  - Cell viability assay
  - Colony formation assay
  - Transwell invasion assay
  - Wound healing assay
  - Immunohistochemical (IHC) analysis
- QUANTIFICATION AND STATISTICAL ANALYSIS
  - Analysis of gene expression by the OmniAnalyzer pro
  - Dimensionality reduction
  - Inferred copy number variation (inferCNV) analysis
  - Diffusion pseudotime (DPT) analysis
  - Partition-based graph abstraction (PAGA) analysis
  - Differentially expressed gene (DEG) analysis
  - Enrichment analysis
  - Bioinformatic analysis using The Cancer Genome Atlas Prostate Adenocarcinoma (TCGA-PRAD) dataset
  - Statistical analysis

SUPPLEMENTAL INFORMATION

Supplemental information can be found online at https://doi.org/10.1016/j.isci.2024.111351.

Received: June 11, 2024
Revised: September 17, 2024
Accepted: November 6, 2024
Published: November 9, 2024

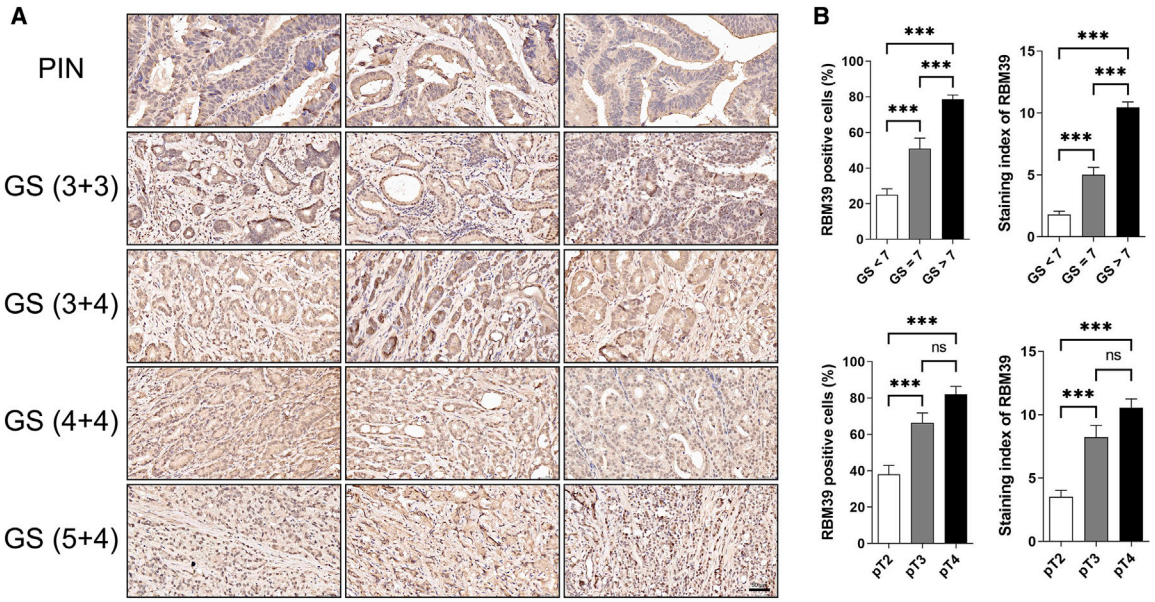

Figure 7. RBM39 protein expression in the clinicopathological characteristics of different GSs and pT stages

(A) Representative images of IHC staining for RBM39 in PCa tissues with different histological types [PIN, GS (3 + 3), GS (3 + 4), GS (4 + 4), and GS (5 + 4)].

(B) Quantitative results of the RBM39 staining percentage and staining index in PCa tissues with different GSs (GS < 7, GS = 7, and GS > 7) and pT stages (pT2, pT3, and pT4) are shown as histograms. The means ± SEMs are displayed in the histograms. ns $p > 0.05$ and *** $p < 0.001$.

REFERENCES

1. Andreoiu, M., and Cheng, L. (2010). Multifocal prostate cancer: biologic, prognostic, and therapeutic implications. Hum. Pathol. *41*, 781–793. https://doi.org/10.1016/j.humpath.2010.02.011.

2. Haffner, M.C., Zwart, W., Roudier, M.P., True, L.D., Nelson, W.G., Epstein, J.I., De Marzo, A.M., Nelson, P.S., and Yegnasubramanian, S. (2021). Genomic and phenotypic heterogeneity in prostate cancer. Nat. Rev. Urol. *18*, 79–92. https://doi.org/10.1038/s41585-020-00400-w.

3. Boyd, L.K., Mao, X., Xue, L., Lin, D., Chaplin, T., Kudahetti, S.C., Stankiewicz, E., Yu, Y., Beltran, L., Shaw, G., et al. (2012). High-resolution genome-wide copy-number analysis suggests a monoclonal origin of multifocal prostate cancer. Genes Chromosomes Cancer *51*, 579–589. https://doi.org/10.1002/gcc.21944.

4. Gundem, G., Van Loo, P., Kremeyer, B., Alexandrov, L.B., Tubio, J.M.C., Papaemmanuil, E., Brewer, D.S., Kallio, H.M.L., Högnäs, G., Annala, M., et al. (2015). The evolutionary history of lethal metastatic prostate cancer. Nature *520*, 353–357. https://doi.org/10.1038/nature14347.

5. Liu, W., Laitinen, S., Khan, S., Vihinen, M., Kowalski, J., Yu, G., Chen, L., Ewing, C.M., Eisenberger, M.A., Carducci, M.A., et al. (2009). Copy number analysis indicates monoclonal origin of lethal metastatic prostate cancer. Nat. Med. *15*, 559–565. https://doi.org/10.1038/nm.1944.

6. Hong, M.K.H., Macintyre, G., Wedge, D.C., Van Loo, P., Patel, K., Lunke, S., Alexandrov, L.B., Sloggett, C., Cmero, M., Marass, F., et al. (2015). Tracking the origins and drivers of subclonal metastatic expansion in prostate cancer. Nat. Commun. *6*, 6605. https://doi.org/10.1038/ncomms7605.

7. Erickson, A., He, M., Berglund, E., Marklund, M., Mirzazadeh, R., Schultz, N., Kvastad, L., Andersson, A., Bergenstråhle, L., Bergenstråhle, J., et al. (2022). Spatially resolved clonal copy number alterations in benign and malignant tissue. Nature *608*, 360–367. https://doi.org/10.1038/s41586-022-05023-2.

8. Goldstein, A.S., Huang, J., Guo, C., Garraway, I.P., and Witte, O.N. (2010). Identification of a cell of origin for human prostate cancer. Science *329*, 568–571. https://doi.org/10.1126/science.1189992.

9. Wang, X., Kruithof-de Julio, M., Economides, K.D., Walker, D., Yu, H., Halili, M.V., Hu, Y.P., Price, S.M., Abate-Shen, C., and Shen, M.M. (2009). A luminal epithelial stem cell that is a cell of origin for prostate cancer. Nature *461*, 495–500. https://doi.org/10.1038/nature08361.

10. Wang, Z.A., Mitrofanova, A., Bergren, S.K., Abate-Shen, C., Cardiff, R.D., Califano, A., and Shen, M.M. (2013). Lineage analysis of basal epithelial cells reveals their unexpected plasticity and supports a cell-of-origin model for prostate cancer heterogeneity. Nat. Cell Biol. *15*, 274–283. https://doi.org/10.1038/ncb2697.

11. Lawson, D.A., Zong, Y., Memarzadeh, S., Xin, L., Huang, J., and Witte, O.N. (2010). Basal epithelial stem cells are efficient targets for prostate cancer initiation. Proc. Natl. Acad. Sci. USA *107*, 2610–2615. https://doi.org/10.1073/pnas.0913873107.

12. Lee, S.H., and Shen, M.M. (2015). Cell types of origin for prostate cancer. Curr. Opin. Cell Biol. *37*, 35–41. https://doi.org/10.1016/j.ceb.2015.10.002.

13. Xin, L. (2013). Cells of origin for cancer: an updated view from prostate cancer. Oncogene *32*, 3655–3663. https://doi.org/10.1038/onc.2012.541.

14. Taylor, R.A., Toivanen, R., Frydenberg, M., Pedersen, J., Harewood, L., Australian Prostate Cancer Bioresource; Collins, A.T., Maitland, N.J., and Risbridger, G.P. (2012). Human epithelial basal cells are cells of origin of prostate cancer, independent of CD133 status. Stem Cell. *30*, 1087–1096. https://doi.org/10.1002/stem.1094.

15. Chen, S., Zhu, G., Yang, Y., Wang, F., Xiao, Y.T., Zhang, N., Bian, X., Zhu, Y., Yu, Y., Liu, F., et al. (2021). Single-cell analysis reveals transcriptomic remodellings in distinct cell types that contribute to human prostate cancer progression. Nat. Cell Biol. *23*, 87–98. https://doi.org/10.1038/s41556-020-00613-6.

16. Dong, B., Miao, J., Wang, Y., Luo, W., Ji, Z., Lai, H., Zhang, M., Cheng, X., Wang, J., Fang, Y., et al. (2020). Single-cell analysis supports a

luminal-neuroendocrine transdifferentiation in human prostate cancer. Commun. Biol. *3*, 778. https://doi.org/10.1038/s42003-020-01476-1.

17. Ma, X., Guo, J., Liu, K., Chen, L., Liu, D., Dong, S., Xia, J., Long, Q., Yue, Y., Zhao, P., et al. (2020). Identification of a distinct luminal subgroup diagnosing and stratifying early stage prostate cancer by tissue-based single-cell RNA sequencing. Mol. Cancer *19*, 147. https://doi.org/10.1186/s12943-020-01264-9.
18. Satija, R., Farrell, J.A., Gennert, D., Schier, A.F., and Regev, A. (2015). Spatial reconstruction of single-cell gene expression data. Nat. Biotechnol. *33*, 495–502. https://doi.org/10.1038/nbt.3192.
19. Achim, K., Pettit, J.B., Saraiva, L.R., Gavriouchkina, D., Larsson, T., Arendt, D., and Marioni, J.C. (2015). High-throughput spatial mapping of single-cell RNA-seq data to tissue of origin. Nat. Biotechnol. *33*, 503–509. https://doi.org/10.1038/nbt.3209.
20. Ke, R., Mignardi, M., Pacureanu, A., Svedlund, J., Botling, J., Wählby, C., and Nilsson, M. (2013). In situ sequencing for RNA analysis in preserved tissue and cells. Nat. Methods *10*, 857–860. https://doi.org/10.1038/nmeth.2563.
21. Lee, J.H., Daugharthy, E.R., Scheiman, J., Kalhor, R., Yang, J.L., Ferrante, T.C., Terry, R., Jeanty, S.S.F., Li, C., Amamoto, R., et al. (2014). Highly multiplexed subcellular RNA sequencing *in situ*. Science *343*, 1360–1363. https://doi.org/10.1126/science.1250212.
22. Berglund, E., Maaskola, J., Schultz, N., Friedrich, S., Marklund, M., Bergenstråhle, J., Tarish, F., Tanoglidi, A., Vickovic, S., Larsson, L., et al. (2018). Spatial maps of prostate cancer transcriptomes reveal an unexplored landscape of heterogeneity. Nat. Commun. *9*, 2419. https://doi.org/10.1038/s41467-018-04724-5.
23. Watanabe, R., Miura, N., Kurata, M., Kitazawa, R., Kikugawa, T., and Saika, T. (2023). Spatial Gene Expression Analysis Reveals Characteristic Gene Expression Patterns of De Novo Neuroendocrine Prostate Cancer Coexisting with Androgen Receptor Pathway Prostate Cancer. Int. J. Mol. Sci. *24*, 8955. https://doi.org/10.3390/ijms24108955.
24. Ståhl, P.L., Salmén, F., Vickovic, S., Lundmark, A., Navarro, J.F., Magnusson, J., Giacomello, S., Asp, M., Westholm, J.O., Huss, M., et al. (2016). Visualization and analysis of gene expression in tissue sections by spatial transcriptomics. Science *353*, 78–82. https://doi.org/10.1126/science.aaf2403.
25. Quan, Y., Zhang, H., Wang, M., and Ping, H. (2023). Visium spatial transcriptomics reveals intratumor heterogeneity and profiles of Gleason score progression in prostate cancer. iScience *26*, 108429. https://doi.org/10.1016/j.isci.2023.108429.
26. Vis, A.N., Roemeling, S., Kranse, R., Schröder, F.H., and van der Kwast, T.H. (2007). Should we replace the Gleason score with the amount of high-grade prostate cancer? Eur. Urol. *51*, 931–939. https://doi.org/10.1016/j.eururo.2006.07.051.
27. Gleason, D.F. (1992). Histologic grading of prostate cancer: a perspective. Hum. Pathol. *23*, 273–279. https://doi.org/10.1016/0046-8177(92)90108-f.
28. Gleason, D.F. (1966). Classification of prostatic carcinomas. Cancer Chemother. Rep. *50*, 125–128.
29. Gleason, D.F., and Mellinger, G.T. (1974). Prediction of prognosis for prostatic adenocarcinoma by combined histological grading and clinical staging. J. Urol. *111*, 58–64. https://doi.org/10.1016/s0022-5347(17)59889-4.
30. Andrén, O., Fall, K., Franzén, L., Andersson, S.O., Johansson, J.E., and Rubin, M.A. (2006). How well does the Gleason score predict prostate cancer death? A 20-year followup of a population based cohort in Sweden. J. Urol. *175*, 1337–1340. https://doi.org/10.1016/s0022-5347(05)00734-2.
31. Humphrey, P.A. (2004). Gleason grading and prognostic factors in carcinoma of the prostate. Mod. Pathol. *17*, 292–306. https://doi.org/10.1038/modpathol.3800054.
32. Lotan, T.L., and Epstein, J.I. (2010). Clinical implications of changing definitions within the Gleason grading system. Nat. Rev. Urol. *7*, 136–142. https://doi.org/10.1038/nrurol.2010.9.
33. Popiolek, M., Rider, J.R., Andrén, O., Andersson, S.O., Holmberg, L., Adami, H.O., and Johansson, J.E. (2013). Natural history of early, localized prostate cancer: a final report from three decades of follow-up. Eur. Urol. *63*, 428–435. https://doi.org/10.1016/j.eururo.2012.10.002.
34. Egevad, L., Granfors, T., Karlberg, L., Bergh, A., and Stattin, P. (2002). Prognostic value of the Gleason score in prostate cancer. BJU Int. *89*, 538–542. https://doi.org/10.1046/j.1464-410x.2002.02669.x.
35. Arora, R., Koch, M.O., Eble, J.N., Ulbright, T.M., Li, L., and Cheng, L. (2004). Heterogeneity of Gleason grade in multifocal adenocarcinoma of the prostate. Cancer *100*, 2362–2366. https://doi.org/10.1002/cncr.20243.
36. Ross, H.M., Kryvenko, O.N., Cowan, J.E., Simko, J.P., Wheeler, T.M., and Epstein, J.I. (2012). Do adenocarcinomas of the prostate with Gleason score (GS) $\leq$6 have the potential to metastasize to lymph nodes? Am. J. Surg. Pathol. *36*, 1346–1352. https://doi.org/10.1097/PAS.0b013e3182556dcd.
37. Donin, N.M., Laze, J., Zhou, M., Ren, Q., and Lepor, H. (2013). Gleason 6 prostate tumors diagnosed in the PSA era do not demonstrate the capacity for metastatic spread at the time of radical prostatectomy. Urology *82*, 148–152. https://doi.org/10.1016/j.urology.2013.03.054.
38. Kweldam, C.F., Wildhagen, M.F., Bangma, C.H., and van Leenders, G.J.L.H. (2015). Disease-specific death and metastasis do not occur in patients with Gleason score $\leq$6 at radical prostatectomy. BJU Int. *116*, 230–235. https://doi.org/10.1111/bju.12879.
39. Eggener, S.E., Berlin, A., Vickers, A.J., Paner, G.P., Wolinsky, H., and Cooperberg, M.R. (2022). Low-Grade Prostate Cancer: Time to Stop Calling It Cancer. J. Clin. Oncol. *40*, 3110–3114. https://doi.org/10.1200/jco.22.00123.
40. Labbate, C.V., Paner, G.P., and Eggener, S.E. (2022). Should Grade Group 1 (GG1) be called cancer? World J. Urol. *40*, 15–19. https://doi.org/10.1007/s00345-020-03583-4.
41. Eggener, S.E., Scardino, P.T., Walsh, P.C., Han, M., Partin, A.W., Trock, B.J., Feng, Z., Wood, D.P., Eastham, J.A., Yossepowitch, O., et al. (2011). Predicting 15-year prostate cancer specific mortality after radical prostatectomy. J. Urol. *185*, 869–875. https://doi.org/10.1016/j.juro.2010.10.057.
42. Kozminski, M.A., Tomlins, S., Cole, A., Singhal, U., Lu, L., Skolarus, T.A., Palapattu, G.S., Montgomery, J.S., Weizer, A.Z., Mehra, R., et al. (2016). Standardizing the definition of adverse pathology for lower risk men undergoing radical prostatectomy. Urol. Oncol. *34*, 415.e1-6. https://doi.org/10.1016/j.urolonc.2016.03.019.
43. Deek, M.P., Van der Eecken, K., Phillips, R., Parikh, N.R., Isaacsson Velho, P., Lotan, T.L., Kishan, A.U., Maurer, T., GAP6 Consortium; and Boutros, P.C., et al. (2021). The Mutational Landscape of Metastatic Castration-sensitive Prostate Cancer: The Spectrum Theory Revisited. Eur. Urol. *80*, 632–640. https://doi.org/10.1016/j.eururo.2020.12.040.
44. Ruiz, C., Lenkiewicz, E., Evers, L., Holley, T., Robeson, A., Kiefer, J., Demeure, M.J., Hollingsworth, M.A., Shen, M., Prunkard, D., et al. (2011). Advancing a clinically relevant perspective of the clonal nature of cancer. Proc. Natl. Acad. Sci. USA *108*, 12054–12059. https://doi.org/10.1073/pnas.1104009108.
45. Robinson, D., Van Allen, E.M., Wu, Y.M., Schultz, N., Lonigro, R.J., Mosquera, J.M., Montgomery, B., Taplin, M.E., Pritchard, C.C., Attard, G., et al. (2015). Integrative clinical genomics of advanced prostate cancer. Cell *161*, 1215–1228. https://doi.org/10.1016/j.cell.2015.05.001.
46. Nowell, P.C. (1976). The clonal evolution of tumor cell populations. Science *194*, 23–28. https://doi.org/10.1126/science.959840.
47. Greaves, M., and Maley, C.C. (2012). Clonal evolution in cancer. Nature *481*, 306–313. https://doi.org/10.1038/nature10762.
48. Yang, X.Q., Jing, X.Y., Zhang, C.X., Song, Y.F., and Liu, D. (2018). Isolation and characterization of porcine PILRB gene and its alternative splicing variants. Gene *672*, 8–15. https://doi.org/10.1016/j.gene.2018.06.008.

49. Tato, C.M., Joyce-Shaikh, B., Banerjee, A., Chen, Y., Sathe, M., Ewald, S.E., Liu, M.R., Gorman, D., McClanahan, T.K., Phillips, J.H., et al. (2012). The myeloid receptor PILRβ mediates the balance of inflammatory responses through regulation of IL-27 production. PLoS One *7*, e31680. https://doi.org/10.1371/journal.pone.0031680.

50. Che, H., Liu, Y., Zhang, M., Meng, J., Feng, X., Zhou, J., and Liang, C. (2019). Integrated Analysis Revealed Prognostic Factors for Prostate Cancer Patients. Med. Sci. Mon. Int. Med. J. Exp. Clin. Res. *25*, 9991–10007. https://doi.org/10.12659/msm.918045.

51. Dowhan, D.H., Hong, E.P., Auboeuf, D., Dennis, A.P., Wilson, M.M., Berget, S.M., and O'Malley, B.W. (2005). Steroid hormone receptor coactivation and alternative RNA splicing by U2AF65-related proteins CAPERalpha and CAPERbeta. Mol. Cell *17*, 429–439. https://doi.org/10.1016/j.molcel.2004.12.025.

52. Tari, M., Manceau, V., de Matha Salone, J., Kobayashi, A., Pastré, D., and Maucuer, A. (2019). U2 AF 65 assemblies drive sequence-specific splice site recognition. EMBO Rep. *20*, e47604. https://doi.org/10.15252/embr.201847604.

53. Han, T., Goralski, M., Gaskill, N., Capota, E., Kim, J., Ting, T.C., Xie, Y., Williams, N.S., and Nijhawan, D. (2017). Anticancer sulfonamides target splicing by inducing RBM39 degradation via recruitment to DCAF15. Science *356*, eaal3755. https://doi.org/10.1126/science.aal3755.

54. Královicová, J., Ševcíková, I., Stejskalová, E., Obuca, M., Hiller, M., Stanek, D., and Vorechovský, I. (2018). PUF60-activated exons uncover altered 3' splice-site selection by germline missense mutations in a single RRM. Nucleic Acids Res. *46*, 6166–6187. https://doi.org/10.1093/nar/gky389.

55. Mai, S., Qu, X., Li, P., Ma, Q., Cao, C., and Liu, X. (2016). Global regulation of alternative RNA splicing by the SR-rich protein RBM39. Biochim. Biophys. Acta *1859*, 1014–1024. https://doi.org/10.1016/j.bbagrm.2016.06.007.

56. Wang, E., Lu, S.X., Pastore, A., Chen, X., Imig, J., Chun-Wei Lee, S., Hockemeyer, K., Ghebrechristos, Y.E., Yoshimi, A., Inoue, D., et al. (2019). Targeting an RNA-Binding Protein Network in Acute Myeloid Leukemia. Cancer Cell *35*, 369–384.e7. https://doi.org/10.1016/j.ccell.2019.01.010.

57. Xu, Y., Nijhuis, A., and Keun, H.C. (2022). RNA-binding motif protein 39 (RBM39): An emerging cancer target. Br. J. Pharmacol. *179*, 2795–2812. https://doi.org/10.1111/bph.15331.

58. Eléouët, M., Lu, C., Zhou, Y., Yang, P., Ma, J., and Xu, G. (2023). Insights on the biological functions and diverse regulation of RNA-binding protein 39 and their implication in human diseases. Biochim. Biophys. Acta. Gene Regul. Mech. *1866*, 194902. https://doi.org/10.1016/j.bbagrm.2022.194902.

59. Liu, L.L., Xie, N., Sun, S., Plymate, S., Mostaghel, E., and Dong, X. (2014). Mechanisms of the androgen receptor splicing in prostate cancer cells. Oncogene *33*, 3140–3150. https://doi.org/10.1038/onc.2013.284.

60. Hu, R., Dunn, T.A., Wei, S., Isharwal, S., Veltri, R.W., Humphreys, E., Han, M., Partin, A.W., Vessella, R.L., Isaacs, W.B., et al. (2009). Ligand-independent androgen receptor variants derived from splicing of cryptic exons signify hormone-refractory prostate cancer. Cancer Res. *69*, 16–22. https://doi.org/10.1158/0008-5472.can-08-2764.

61. Dehm, S.M., Schmidt, L.J., Heemers, H.V., Vessella, R.L., and Tindall, D.J. (2008). Splicing of a novel androgen receptor exon generates a constitutively active androgen receptor that mediates prostate cancer therapy resistance. Cancer Res. *68*, 5469–5477. https://doi.org/10.1158/0008-5472.can-08-0594.

62. Melnyk, J.E., Steri, V., Nguyen, H.G., Hann, B., Feng, F.Y., and Shokat, K.M. (2020). The splicing modulator sulfonamide indisulam reduces AR-V7 in prostate cancer cells. Bioorg. Med. Chem. *28*, 115712. https://doi.org/10.1016/j.bmc.2020.115712.

63. Greene, J., Baird, A.M., Casey, O., Brady, L., Blackshields, G., Lim, M., O'Brien, O., Gray, S.G., McDermott, R., and Finn, S.P. (2019). Circular RNAs are differentially expressed in prostate cancer and are potentially associated with resistance to enzalutamide. Sci. Rep. *9*, 10739. https://doi.org/10.1038/s41598-019-47189-2.

64. Jung, D.J., Na, S.Y., Na, D.S., and Lee, J.W. (2002). Molecular cloning and characterization of CAPER, a novel coactivator of activating protein-1 and estrogen receptors. J. Biol. Chem. *277*, 1229–1234. https://doi.org/10.1074/jbc.M110417200.

65. Dutta, J., Fan, G., and Gélinas, C. (2008). CAPERalpha is a novel Rel-TAD-interacting factor that inhibits lymphocyte transformation by the potent Rel/NF-kappaB oncoprotein v-Rel. J. Virol. *82*, 10792–10802. https://doi.org/10.1128/jvi.00903-08.

66. Kang, Y.K., Putluri, N., Maity, S., Tsimelzon, A., Ilkayeva, O., Mo, Q., Lonard, D., Michailidis, G., Sreekumar, A., Newgard, C.B., et al. (2015). CAPER is vital for energy and redox homeostasis by integrating glucose-induced mitochondrial functions via ERR-α-Gabpa and stress-induced adaptive responses via NF-κB-cMYC. PLoS Genet. *11*, e1005116. https://doi.org/10.1371/journal.pgen.1005116.

67. Zhou, J., Simon, J.M., Liao, C., Zhang, C., Hu, L., Zurlo, G., Liu, X., Fan, C., Hepperla, A., Jia, L., et al. (2022). An oncogenic JMJD6-DGAT1 axis tunes the epigenetic regulation of lipid droplet formation in clear cell renal cell carcinoma. Mol. Cell *82*, 3030–3044.e8. https://doi.org/10.1016/j.molcel.2022.06.003.

68. Puvvula, P.K., Yu, Y., Sullivan, K.R., Eyob, H., Rosenberg, J., Welm, A., Huff, C., and Moon, A.M. (2021). Inhibiting an RBM39/MLL1 epigenomic regulatory complex with dominant-negative peptides disrupts cancer cell transcription and proliferation. Cell Rep. *35*, 109156. https://doi.org/10.1016/j.celrep.2021.109156.

69. Chilewski, S.D., Bhosale, D., Dees, S., Hutchinson, I., Trimble, R., Pontiggia, L., Mercier, I., and Jasmin, J.F. (2020). Development of CAPER peptides for the treatment of triple negative breast cancer. Cell Cycle *19*, 432–447. https://doi.org/10.1080/15384101.2020.1711579.

70. Quan, Y., Zhang, X., Butler, W., Du, Z., Wang, M., Liu, Y., and Ping, H. (2021). The role of N-cadherin/c-Jun/NDRG1 axis in the progression of prostate cancer. Int. J. Biol. Sci. *17*, 3288–3304. https://doi.org/10.7150/ijbs.63300.

71. Yu, G., Wang, L.G., Han, Y., and He, Q.Y. (2012). clusterProfiler: an R package for comparing biological themes among gene clusters. OMICS *16*, 284–287. https://doi.org/10.1089/omi.2011.0118.

72. Wu, T., Hu, E., Xu, S., Chen, M., Guo, P., Dai, Z., Feng, T., Zhou, L., Tang, W., Zhan, L., et al. (2021). clusterProfiler 4.0: A universal enrichment tool for interpreting omics data. Innovation *2*, 100141. https://doi.org/10.1016/j.xinn.2021.100141.

73. Ritchie, M.E., Phipson, B., Wu, D., Hu, Y., Law, C.W., Shi, W., and Smyth, G.K. (2015). limma powers differential expression analyses for RNA-sequencing and microarray studies. Nucleic Acids Res. *43*, e47. https://doi.org/10.1093/nar/gkv007.

74. Quan, Y., Zhang, X., and Ping, H. (2022). Construction of a risk prediction model using m6A RNA methylation regulators in prostate cancer: comprehensive bioinformatic analysis and histological validation. Cancer Cell Int. *22*, 33. https://doi.org/10.1186/s12935-021-02438-1.

75. Liu, J., Lichtenberg, T., Hoadley, K.A., Poisson, L.M., Lazar, A.J., Cherniack, A.D., Kovatich, A.J., Benz, C.C., Levine, D.A., Lee, A.V., et al. (2018). An Integrated TCGA Pan-Cancer Clinical Data Resource to Drive High-Quality Survival Outcome Analytics. Cell *173*, 400–416.e11. https://doi.org/10.1016/j.cell.2018.02.052.

STAR★METHODS

KEY RESOURCES TABLE

REAGENT or RESOURCE	SOURCE	IDENTIFIER
Antibodies		
RBM39	Abcam	Cat# ab25801; RRID: AB_2936825
β-actin	Cell Signaling Technology (CST)	Cat# 3700; RRID: AB_2242334
Biological samples		
Prostate cancer (PCa) tissues	Beijing Tongren Hospital	N/A
Critical commercial assays		
Visium Spatial Gene Expression Slide & Reagent kit	10x Genomics	V10N30-034
Visium Spatial Tissue Optimization Slide & Reagent kit	10x Genomics	201012
TRIzol reagent	Invitrogen	Cat# 15596018
One-Step gDNA Removal and cDNA Synthesis SuperMix	TransGen Biotech	AE311-03
Top Green qPCR SuperMix	TransGen Biotech	AQ131-04
Radioimmunoprecipitation assay (RIPA) buffer	Solarbio	R0020
BCA protein assay kit	KeyGen Biotech	KGP902
Polyvinylidene difluoride (PVDF) membrane	Merck Millipore	03010040001
Chemiluminescent HRP Substrate	Merck Millipore	WBKLS0500
Fetal bovine serum (FBS) and mediums	This paper	N/A
Cell Counting Kit-8 (CCK-8)	MedChemExpress (MCE)	Cat# HY-K0301
Crystal violet solution	Beyotime	C0121
Transwell chambers	Corning	3422
Matrigel	BD Biosciences	356234
Deposited data		
PCa in The Cancer Genome Atlas (TCGA)	TCGA Genomic Data Commons (GDC) Data Portal	https://portal.gdc.cancer.gov/
Progression-free survival (PFS) data	University of California Santa Cruz (UCSC) Xena website	https://xenabrowser.net/datapages/
Visium spatial transcriptomics (ST) data	Quan et al.[25]	Science Data Bank (ScienceDB): https://doi.org/10.57760/sciencedb.09389 and https://cstr.cn/31253.11.sciencedb.09389
Experimental models: Cell lines		
C4-2	ATCC	CRL-3314
PC3	ATCC	CRL-1435
DU145	ATCC	HTB-81
Oligonucleotides		
Gene regulation related sequences, see Table S1	This paper	N/A
Primers used for qPCR, see Table S2	This paper	N/A
Software and algorithms		
cellSens Dimension Software	Olympus	N/A
10x Genomics Visium library preparation protocol	10x Genomics	200100
Space Ranger	10x Genomics	N/A
OmniAnalyzer Pro	Abiosciences	N/A
Singular value decomposition (SVD)	OmniAnalyzer Pro	N/A

(*Continued on next page*)

Continued

REAGENT or RESOURCE	SOURCE	IDENTIFIER
Uniform manifold approximation and projection (UMAP)	OmniAnalyzer Pro	N/A
Seurat	OmniAnalyzer Pro	N/A
Inferred copy number variation (inferCNV)	OmniAnalyzer Pro	N/A
Diffusion pseudotime (DPT)	OmniAnalyzer Pro	N/A
Partition-based graph abstraction (PAGA)	OmniAnalyzer Pro	N/A
Differentially expressed gene (DEG) analysis	OmniAnalyzer Pro	N/A
R software (Version 4.0.3)	the R Core Team and the R Foundation for Statistical Computing	https://www.r-project.org/
clusterProfiler	R package, G Yu et al.[71,72]	https://bioconductor.org/packages/release/bioc/html/clusterProfiler.html
enrichplot	R package	https://bioconductor.org/packages/release/bioc/html/enrichplot.html
limma	R package, Ritchie ME et al.[73]	https://bioconductor.org/packages/release/bioc/html/limma.html
reshape2	R package	https://cran.r-project.org/web/packages/reshape2/index.html
ggpurb	R package	https://cran.r-project.org/web/packages/ggpubr/index.html
survival	R package	https://cran.r-project.org/web/packages/survival/index.html
survminer	R package	https://cran.r-project.org/web/packages/survminer/index.html
VennDiagram	R package	https://cran.r-project.org/web/packages/VennDiagram/index.html
grid	R package	https://cran.r-project.org/web/packages/grid/index.html
futile.logger	R package	https://cran.r-project.org/web/packages/futile.logger/index.html
formatR	R package	https://cran.r-project.org/web/packages/formatR/index.html
ChemiDoc™ XRS+ with Image Lab™ software	Bio-Rad	N/A
Microsoft Excel 2019 software	Microsoft Corp.	N/A
GraphPad Prism 9.0.0	Dotmatics	https://www.graphpad.com/

EXPERIMENTAL MODEL AND STUDY PARTICIPANT DETAILS

Preparation of prostate cancer (PCa) tissues

For spatial transcriptomics (ST) analysis, PCa tissue with a Gleason score (GS) of 3+4 was collected from a single patient after radical prostatectomy. Patient information is shown in Table 1. The excision site was selected according to the pathological diagnosis of the prostate biopsy. The fresh tissue was snap-frozen on dry ice, embedded in freezing and Optimal Cutting Temperature (OCT) compound, cryosectioned into 10 μm sections, and placed on Visium Spatial slides.

For histological analysis, forty-five PCa patients who underwent prostatectomy were recruited, and PCa and prostatic intraepithelial neoplasia (PIN) tissues were extracted and paraffin-embedded until use. The clinicopathological information of these patients is presented in Table 2.

Cell culture

The C4-2, PC3, and DU145 cell lines were obtained from the American Type Culture Collection (Rockville, MD, USA). The cells were cultured in Roswell Park Memorial Institute (RPMI) 1640 medium or Dulbecco's modified Eagle medium (DMEM) (Gibco, Grand Island, NY, USA), supplemented with 10% fetal bovine serum (FBS) (HyClone, South Logan, UT, USA) and 1% antibiotic-antimycotic (Gibco, Grand Island, NY, USA) in a humidified atmosphere at 37°C and 5% CO_2.

Ethical statement

Human prostate tissue samples were obtained from Beijing Tongren Hospital. Ethical consent was obtained from the Ethics Committee of Beijing Tongren Hospital, which is affiliated with Capital Medical University.

METHOD DETAILS

Visium spatial transcriptomics (ST)

The Visium Spatial Gene Expression Slide & Reagent Kit (10× Genomics, CA, USA) was used according to the manufacturer's instructions to generate spatially barcoded cDNA from the tissue section. The polyadenylated mRNAs released from the overlying PCa cells were subjected to reverse transcription, cDNA synthesis, and polymerase chain reaction (PCR) amplification. A Visium Spatial Tissue Optimization Slide with a PCa tissue section was subjected to methanol fixation and hematoxylin–eosin (H&E) staining. In the quality control experiment, the permeabilization condition for the tissue section was optimized by utilizing the Visium Spatial Tissue Optimization Slide & Reagent Kit (10× Genomics) according to the manufacturer's instructions. The optimal permeation time in this section was 18 min, which is the standard for penetration operation. Libraries for PCa section was generated on the basis of the 10x Genomics Visium library preparation protocol, and 150PE-mode sequencing was carried out on the Illumina NovaSeq600 platform (Illumina, CA, USA). Space Ranger (10× Genomics) was used to perform splicing-aware alignment of reads to the genome though an aligner called STAR.

Gene regulation in PCa cell lines

To stably downregulate RBM39, lentiviruses harboring specific short hairpin RNA (shRNA) sequences were generated by GENECHEM (Shanghai, China). PCa cells were infected with lentiviruses containing 5 μg/ml polybrene, and successfully transduced cells were selected with 1–2 μg/ml puromycin. The sequence of the RBM39 shRNA is shown in Table S1.

Reverse transcription (RT) and quantitative real-time PCR (qPCR) analysis

RNA isolation, complementary DNA (cDNA) synthesis, and qPCR were conducted using TRIzol™ reagent (Invitrogen, Carlsbad, CA, USA), One-Step gDNA Removal and cDNA Synthesis SuperMix (TransGen Biotech, Beijing, China) with anchored oligo (dT) primers, and Top Green qPCR SuperMix (TransGen Biotech) on an SDS 7500 FAST Real-Time PCR system (Applied Biosystems, Foster City, CA, USA), following to the manufacturer's instructions. The endogenous reference genes GAPDH and 18S ribosomal RNA were used for normalization. The relevant primer sequences are shown in Table S2.

Western blotting (WB)

Protein extraction and quantification were performed with radioimmunoprecipitation assay (RIPA) buffer (Solarbio, Beijing, China) and a BCA protein assay kit (KeyGen Biotech, Nanjing, China). The proteins were separated using SDS–polyacrylamide gel electrophoresis (SDS–PAGE) and transferred to polyvinylidene difluoride (PVDF) membranes (Merck Millipore, Billerica, MA, USA). After incubation with primary and secondary antibodies, the immunoreactive bands on the membranes were detected through the use of Chemiluminescent HRP Substrate (Merck Millipore) and ChemiDoc™ XRS+ with Image Lab™ software (Bio-Rad, Hercules, CA, USA). Antibodies against RBM39 (ab25801; Abcam, Cambridge, MA, USA) and β-actin (Cat# 3700; Cell Signaling Technology (CST), Danvers, MA, USA) were used in this study (Table S3).

Cell viability assay

A total of 2×10^3 cells were seeded in 96-well plates and cultured for 2 to 4 days. At the indicated time points, cell viability was determined using Cell Counting Kit-8 (CCK-8) (MedChemExpress (MCE), Monmouth Junction, NJ, USA) assays according to the manufacturer's instructions.

Colony formation assay

A total of 2×10^3 cells were evenly seeded in 6-well plates and cultured for 2 weeks to allow visible colony formation. Then, the cells were stained with 0.01% crystal violet solution (Beyotime, Shanghai, China) and fully decolorized.

Transwell invasion assay

Transwell chambers (Corning, NY, USA) were used to detect cell invasion. The membrane of the upper chamber was coated with Matrigel (BD Biosciences, San Jose, CA, USA), and 5×10^4 cells were seeded in serum-free medium. The lower chamber was filled with a chemoattractant of 20% FBS in 500 μl of medium. After incubation for 2 days, the cells on the upper surface of the transwell membranes were removed, and the remaining cells were stained with 0.01% crystal violet solution (Beyotime, Shanghai, China).

Wound healing assay

A wound healing assay was performed to evaluate cell migration. A total of 5×10^5 cells were seeded in 6-well plates, and a scratch was generated by a 200-μl pipette tip in the middle of each well. Cell migration was imaged via light microscopy at the indicated time points.

Immunohistochemical (IHC) analysis

For IHC analysis, PCa tissues were paraffin-embedded and sectioned at 5 μm. The sections were subjected to antigen retrieval and incubated with target primary and secondary antibodies. An antibody against RBM39 (ab25801; Abcam, Cambridge, MA, USA) was used in this study (Table S3).

For statistical analysis, we selected representative slides at 36.4× magnification and assigned each a staining intensity score (1 for weak, 2 for moderate, and 3 for strong) and a staining percentage score (0 for $\leq$ 5% positive cells; 1 for 6–25% positive cells; 2 for 26–50% positive cells; 3 for 51–75% positive cells; and 4 for $\geq$ 76% positive cells). The staining index (SI) was then calculated by multiplying the staining intensity score by the staining percentage score.

QUANTIFICATION AND STATISTICAL ANALYSIS

Analysis of gene expression by the OmniAnalyzer pro

OmniAnalyzer Pro [Analytical BioSciences Limited (Abiosciences), Beijing, China] was used to analyze transcriptomes at spatial dimensions, employing an algorithm developed by Scanpy and Abiosciences. The spatial barcode information and reads in each spot were combined, followed by quality control steps involving spot and gene filtering. The data were then normalized to ensure uniform total expression across all spots and subsequently transformed using the natural logarithm [ln (1+normalized value)] to achieve a more normal distribution and minimize the influence of highly expressed genes.

Dimensionality reduction

To reduce the dimensionality of the spatial features based on the expression patterns of highly variable genes (HVGs) (with a minimum mean value of 0.0125, a maximum mean value of 3, a minimum dispersion of 0.5, and a maximum dispersion of 1000), principal component analysis (PCA) (https://scikit-learn.org/stable/modules/generated/sklearn.decomposition.PCA.html) was performed via OmniAnalyzer Pro. The pipeline uses the scipy.sparse.linalg ARPACK implementation of the truncated singular value decomposition (SVD). The PCA number of components is 50 in the filtered data. To visualize the data in a two-dimensional space, the PCA-reduced data were subsequently passed to uniform manifold approximation and projection (UMAP) algorithm. Louvain clustering analysis was performed to divide all the spots into different groups. These classified clusters were indicated by different colors to allow simultaneous visualization of the transcriptome-wide patterns and histological characteristics of all the clusters.

Inferred copy number variation (inferCNV) analysis

The somatic large-scale chromosomal CNVs were inferred from transcriptomic data using the Python reimplementation of inferCNV (https://infercnvpy.readthedocs.io/en/latest/infercnv.html). The transcription intensity of genes across genomic positions was calculated for each spot in comparison to the reference spots within the GS (3+3) cluster.

Diffusion pseudotime (DPT) analysis

DPT analysis was performed to reconstruct the PCa developmental progression of a biological process from snapshot data (https://scanpy.readthedocs.io/en/stable/generated/scanpy.tl.dpt.html). The geodesic graphs generated via this approach were used to identify transient or metastable states, branching decisions and differentiation endpoints.

Partition-based graph abstraction (PAGA) analysis

PAGA maps both discrete disconnected and continuous connected cell-to-cell variations. It can predict PCa developmental trajectories using a transcriptome dataset. An interpretable abstracted graph-like map (PAGA graph) was generated by quantifying the connectivity of different clusters to trajectory inference. The specific method and algorithms used are detailed at https://scanpy.readthedocs.io/en/stable/generated/scanpy.tl.paga.html.

Differentially expressed gene (DEG) analysis

OmniAnalyzer Pro and R software (4.3.1) were used for DEG analysis. The DEGs between two or more clusters were identified through the Wilcoxon test, and the results are shown in volcano plots and Venn diagrams. An absolute value of natural logarithm fold change ($|\ln FC| > 0.1$ and q-value [the false discovery rate (FDR) as calculated by the Benjamini–Hochberg procedure] < 0.001 according to the Wilcoxon test was considered to indicate heterogeneity of gene expression in these comparisons.

Enrichment analysis

R software (4.3.1) was used for enrichment analysis. The biological functions related to the DEGs were assessed through Gene Ontology (GO) and Kyoto Encyclopedia of Genes and Genomes (KEGG) enrichment analyses using the R packages ‘‘clusterProfiler’’ and ‘‘enrichplot’’.

Bioinformatic analysis using The Cancer Genome Atlas Prostate Adenocarcinoma (TCGA-PRAD) dataset

The DEGs identified through ST analysis were validated using the transcripts per kilobase of exon model per million (TPM) values of genes in patients from TCGA-PRAD which were stratified on the basis of clinicopathological characteristics, such as GS, pathological

T stage (pT), and TP53 mutation status. The TCGA-PRAD data and corresponding follow-up phenotype files were downloaded from the Genomic Data Commons (GDC) Data Portal (https://portal.gdc.cancer.gov/). R software (4.3.1) along with the packages "limma", "reshape2", and "ggpubr" were used in this analysis.

To evaluate prognosis influenced by DEGs in clinical outcomes of recurrence-free survival (RFS) and progression-free survival (PFS), Kaplan–Meier (K–M) survival curve analysis and Cox regression analysis were conducted using the R packages "survival" and "survminer". The RFS information was extracted from the phenotype information as previously described,[74] and the PFS data were obtained from the University of California Santa Cruz (UCSC) Xena website (https://xenabrowser.net/datapages/).[75] The intersecting DEGs identified in the above analyses were integrated into a Venn diagram through the R packages "VennDiagram", "grid", "futile.logger", and "formatR".

Statistical analysis

Statistical analysis was performed using OmniAnalyzer Pro, R software (4.0.3), SPSS software version 23 (IBM, Armonk, New York, USA), Microsoft Excel 2019 software (Microsoft Corp., Redmond, WA, USA), and GraphPad Prism 9.0.0 (GraphPad Software, San Diego, CA, USA). The Wilcoxon test with p- or q-value calculations was used to analyze continuous data. Comparisons among $\geq$ 3 groups were performed using the Kruskal–Wallis test or one-way and two-way analysis of variance (ANOVA), followed by post hoc Tukey's or Dunn's multiple comparisons tests. K–M curves with a log-rank test and univariate Cox regression models with hazard ratios (HRs) were generated for survival analyses. A p- or q-value < 0.05 was considered to indicate statistical significance.